IOP Conference Series: Materials Science and Engineering

Pressure-induced critical current reduction in impregnated Nb_3Sn Rutherford cables for use in future accelerator magnets

IOP Conf. Series: Materials Science and Engineering **756** (2020) 012015 doi:10.1088/1757-899X/756/1/012015

Pressure-induced critical current reduction in impregnated Nb_3Sn Rutherford cables for use in future accelerator magnets

P. Gao[1], M. Dhallé[1] and H. H. J. ten Kate[1,2]

[1] University of Twente, Faculty of Science & Technology, Energy, Materials and Systems (EMS), P.O. Box 217, 7500 AE Enschede, The Netherlands

[2] CERN, European Organization for Nuclear Research, 1211 Geneva 23, Switzerland

p.gao@utwente.nl

Abstract. The measured critical current reduction in Nb_3Sn Rutherford cables under magnet-relevant transverse pressure levels is analyzed in terms of the strain state of the filaments inside their strands. Several straightforward mechanical 2D FE models of the cables' cross-section are used to translate the stress that is applied to the surface of the impregnated cables into a strain distribution on its strands. The resulting critical current reduction of the cable is then estimated from the average deviatoric strain in the strands' filamentary zone, using the well-established strain scaling relations obtained for isolated strands. This allows to identify the main factors that influence the pressure response of impregnated Nb_3Sn accelerator cables. The analysis is presented for state-of-the-art cable samples that were measured at the University of Twente and shows how especially stiff and incompressible resins reduces the deviatoric strain in the filamentary zone of the cable strands, but also how relatively small alignment errors can lead to stress concentrations that reduce the critical current density significantly.

1. Introduction

Future circular accelerators such as HL-LHC, FCC or SppC call for bending magnets that generate fields of 16 T or above [1, 2] and will therefore have to rely on Nb_3Sn or HTS technology. This paper focusses on the mechanical stress tolerance of Nb_3Sn Rutherford cables for such magnets. 16 T magnet lay-outs ranging from 'classical' cos-theta [3, 4] over block [5] and common-coil [6] to canted-cos-theta [7] have been proposed, but all involve unprecedented peak transverse pressure levels in the range of about 140 to 200 MPa on their cables, which operate at non-Cu current densities J_c of about 1500 A/mm^2.

The superconducting properties of Nb_3Sn are well-documented [8] and a-priori understood [9] to change under mechanical strain ε, leading to an intrinsic and reversible J_c reduction at lower strain levels [10] and an irreversible microstructural J_c degradation due to filament cracking when an 'irreversible strain limit' is exceeded [11]. The strain dependence of J_c in the reversible regime is often described as:

$$J_c(T,B,\varepsilon) = \frac{C_1}{B} s(\varepsilon_{dev})(1-t^{1.52})(1-t^2)b^p(1-b)^q\,, \quad (1)$$

with t and b the reduced temperature T/T_c and the reduced magnetic field B/B_{c2}, respectively; C_1, p and q are material-specific fitting parameters and $s(\varepsilon_{dev})$ the strain function [8]. The 'deviatoric strain' ε_{dev} is the square root of the second strain invariant [12], which essentially describes the distortion of the crystal lattice.

To minimize such distortion, and the corresponding reversible J_c reduction, Nb_3Sn strands [13, 14] and cables [15, 16] can be resin-impregnated, which causes a distribution of transverse stresses more evenly and leads to a strongly improved stress tolerance [17]. In this paper we use a number of straightforward FE models to illustrate semi-quantitatively how the resin properties, winding pack composition and detailed layout of the cable confinement influence the transverse pressure tolerance of impregnated Rutherford cables.

2. 2D mechanical models and results

2.1. Influence of the epoxy properties on the deviatoric strain

The isotropic 2D two-strand plane-strain COMSOL model presented in Figure 1 is a simplified simulation of the 'hair-pin' sample holder that is used at the University of Twente in transverse pressure experiments on accelerator-relevant superconducting cables [18]. The strands are initially modelled as homogenous Nb_3Sn cylinders with a diameter of 1 mm that are fully surrounded by an epoxy resin. This uniform-strand assumption will be relaxed later. According to the material properties of the CTD-101K and the composite of CTD-101K + glass-sleeve [19]. The Young's modulus and Poisson's ratio of resin are assumed to be varied in the ranges of 1 to 40 GPa and 0.1 to 0.4, respectively. A normal pressure of 100 MPa is applied to the top of the impregnated sample over a section of 1.2×46 mm^2 with a stainless-steel anvil. The total thickness of the impregnated stack is 2.6 mm, with a distance of 0.1 mm in-between the two strands. The assumed mechanical properties of various materials at 4.2 K are presented in Table 1. The bottom edge of the epoxy is fixed, the left and right sides of the stack and of the anvil are modelled as 'sliding boundaries', which implies that no displacement in horizontal direction can occur at these sides.

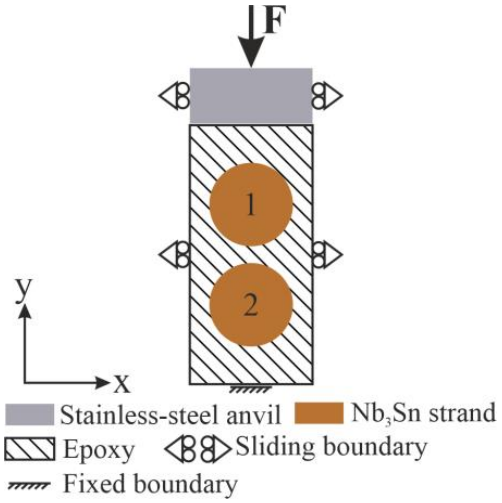

Figure 1. 2D mechanical model comprising a stack of two Nb_3Sn strands.

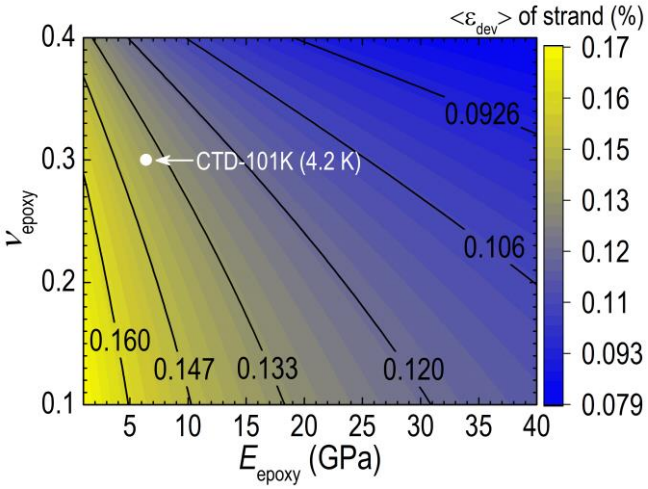

Figure 2. Variation of average deviatoric strain acting on strand-1 with respect to the Young's modulus and the Poisson's ratio of the epoxy resin.

Table 1: MECHANICAL PROPERTIES OF VARIOUS MATERIALS USED IN THE 2-STRAND MODEL.

T = 4.2 K	E (GPa)	ν
Nb_3Sn	75 [20]	0.36 [21]
Epoxy	1 to 40	0.1 to 0.4
Stainless steel 316L	207 [20]	0.284 [20]

Because of the symmetry in the model, only the average deviatoric strain $<\varepsilon_{dev}>$ acting on strand-1 needs to be calculated and is presented in Figure 2 as a function of the Young's modulus E_{epoxy} and the Poisson's ratio ν_{epoxy} of the epoxy resin. With increasing Young's modulus and Poisson's ratio, $<\varepsilon_{dev}>$ decreases. This can be understood intuitively: as the epoxy becomes stiffer (larger E_{epoxy}) it carries a

larger fraction of the applied force and the stress exerted on the strand becomes smaller, causing a corresponding reduction of the strain in the strand. A larger Poisson's ratio of the epoxy resin on the other hand increases its bulk modulus [12], Equation (2), and thus renders the stress distribution more hydrostatic:

$$k_{epoxy} = \frac{E_{epoxy}}{3(1-2\nu_{epoxy})}. \quad (2)$$

Correspondingly, the *x*- and *y*-strains inside the strand become more similar, which also results in a reduction of $<\varepsilon_{dev}>$. It can thus be concluded that using an epoxy resin with either a large Young's modulus or a large Poisson's ratio reduces the deviatoric strain component acting on the strand and hence increases its critical current. In the transverse pressure experiments on Nb_3Sn Rutherford cables [17], the epoxy resin CTD-101K [22] is used, with a reported Young's modulus E_{epoxy} of 6.44 GPa and a Poisson's ratio ν_{epoxy} of 0.3 at 4.2 K [19]. These values are indicated by the dot in Figure 2.

2.2. Influence of glass reinforcement on the deviatoric strain

Vacuum impregnation with epoxy resin is commonly applied in accelerator magnets to enhance the coils' mechanical properties. For large-scale magnets, the epoxy resin CTD-101K is often used due to its long pot life of 60 h and low viscosity 400 mPa.s at 40 °C [20]. In addition, a woven glass sleeve is often applied around the cables to ensure adequate electrical turn-to-turn isolation. As added advantages, compared to the pure epoxy resin the combination of CTD-101K and glass fibers has a thermal contraction coefficient that is closer to the one of the Nb_3Sn cables, as well as a larger Young's modulus. The orthotropic mechanical properties of the glass-resin composite are presented in Table 2.

Table 2. MECHANICAL PROPERTIES OF CTD-101K WITH AN S-2 GLASS-FIBER SLEEVE [19].

T = 4.2 K	E_x / E_y / E_z (GPa)	ν_x / ν_y / ν_z	G_x / G_y / G_z (GPa)
CTD-101K & glass-fiber	39.4 / 19.7 / 32.9	0.21 / 0.12 / 0.22	9 / 4.9 / 9

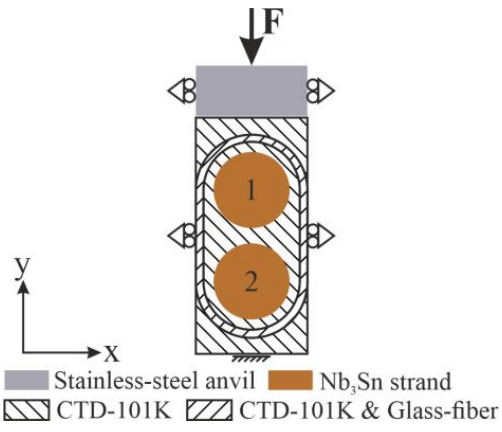

Figure 3. 2-strand model including epoxy resin & woven glass sleeve.

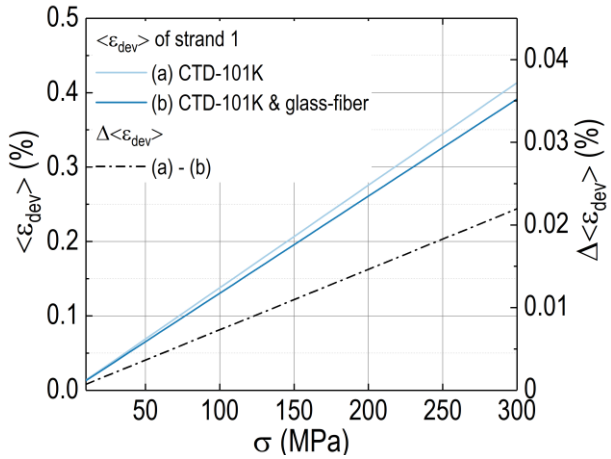

Figure 4. Average deviatoric strain acting on strand-1 with and without glass sleeve (left axis) and the difference between both (right axis) plotted against the applied pressure.

We can adapt the simple cable model of Figure 1 to include the glass and thus to estimate the change in the average deviatoric strain in the strand due to the presence of the sleeve. The resulting 2D mechanical model is presented in Figure 3. It has the same size and boundary constraints as the 2-strand model of Figure 1, but this time the medium enclosing the strands has three different regions: the pure epoxy resin outside the sleeve, the resin mixed with glass fibers and the pure resin inside the sleeve. The thickness of the sleeve is taken 50 μm, and the minimum distance between glass-fiber and strand is also

50 μm. As before, transverse pressure is applied to the top surface of the impregnated sample stack through the anvil.

The average deviatoric strain $<\varepsilon_{dev}>$ acting on strand-1 with and without the sleeve is plotted against applied pressure in Figure 4. The difference in deviatoric strain with and without glass is proportional to the applied pressure, with the strands in the sample impregnated with CTD-101K mixed with glass-fiber experiencing a 5% lower average deviatoric strain compared to the sample impregnated with pure CTD-101K.

2.3. Influence of the confinement geometry on the deviatoric strain (effect of the alignment impregnation)

As reported elsewhere [17], a first series of critical current versus transverse pressure measurements on Rutherford cables for the Short Model Coil (SMC) demonstrator magnet program at CERN (comprising 18 Restacked-Rod-Processed (RRP) or Powder-In-Tube (PIT) Nb_3Sn strands) yielded an irreversible pressure limit of 170 ± 25 MPa for the RRP cable and 125 ± 10 MPa for the PIT cable, which was considerably lower than expected. A possible reason for these low values was a suspected misalignment between the impregnated cable and the pressure anvil. The measurements were repeated on a second set of cable samples with an additional 'alignment impregnation' step [18, 23] to improve the interface parallelism. As a result, the measured transverse pressure tolerance of these two cable types improved significantly, to an irreversible pressure limit larger than 190 ± 3 and 150 ± 3 MPa, respectively.

To estimate how significant the effect of misalignment is on the deviatoric strain in the strands of the measured Nb_3Sn cables, as well as to understand better how the alignment impregnation improves the transverse stress tolerance of the cables, a 2D mechanical model for impregnated cables was developed, as shown in Figure 3. Just like in the previous models, a constant force is applied to the stainless steel anvil while the left and right boundaries of both the anvil and the impregnated cable sample are defined as sliding. Also like in the models above, the strands are still represented by uniform Nb_3Sn cylinders. The input variable d_s in the COMSOL simulations is the vertical displacement of the anvil, while g_s is the initial vertical gap that is left on the "non-touching" edge of the cable when d_s is zero (i.e. when the anvil first comes into contact with the sample at the other edge). θ is the misalignment angle between the anvil and the sample surface.

The various geometrical parameters of the cable model of Figure 5 are summarized in Table 3. The 1 mm diameter strands are surrounded by pure CTD-101K epoxy resin. The minimum distance $d_{c.i}$ between strands and the glass sleeve is 50 μm. Within one layer of strands, neighboring strands are separated by a distance d_a of 50 μm, while the vertical distance d_c between the strands in different layers is 100 μm. This structure is enveloped in a glass sleeve with a thickness $t_{c.g}$ of 50 μm. An additional 100 μm thick pure epoxy resin layer is assumed outside the glass at the top and the bottom of the resulting sample stack. Nb_3Sn, epoxy resin and glass-fiber properties are taken to be the same as in the previous models, as listed in Tables 1 and 2.

Figure 6 shows the calculated average deviatoric strain acting on the strands in the top layer of the cable for a perfectly aligned experiment ($\theta = 0°$) and for an experiment with a small misalignment angle ($\theta = 0.2°$). In both cases, the force applied by the anvil is 20 kN, corresponding to a nominal pressure of 40 MPa. Strikingly, in the misaligned case the deviatoric strain in strand 9, the strand situated directly below the 'first contact' area of the anvil, is about 3 to 3.5 times higher than in the 'perfect' experiment. As we move from the right to the left, from strand 9 to strand 3 in Figure 5, the deviatoric strain decreases approximately linearly. For the left-most strands 1 and 2 the strain becomes less position-dependent. These observations can be understood in terms of the system's geometry, as sketched in Figure 7. For a non-zero misalignment and relatively low anvil displacement d_s, only part of the anvil is in contact with the sample, with an "overall" strain $\varepsilon_y(x)$ that decreases linearly from right to left over the width of the contact area w_c. As long as $d_s < g_s$, w_c will be smaller than the sample width and a gap remains between the anvil and the sample on the left-hand side.

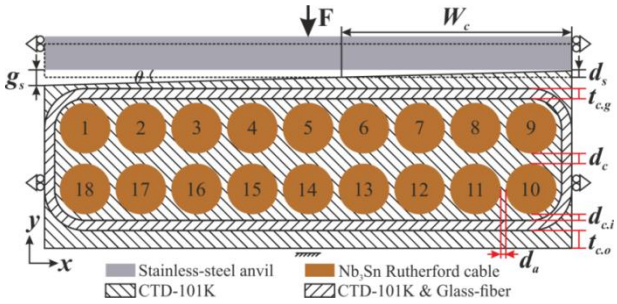

Figure 5. 2D mechanical model of the cable under transverse pressure that includes a misaligned interface.

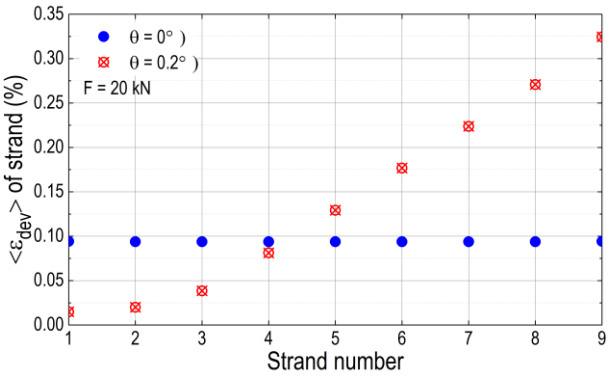

Figure 6. Average deviatoric strain in strands 1 to 9 of the top cable face in Figure 5. The blue solid symbols are modelled assuming perfect parallelism between cable and pressure anvil, the red crossed ones with a small misalignment angle of 0.2°.

Table 3. DIMENSIONAL PARAMETERS OF THE 2D MECHANICAL MODEL OF THE CABLE ARCHITECTURE.

Parameter	Description	Unit	Value
r	Radius of the strand	mm	0.5
$t_{c.o}$	Thickness of the outer CTD-101K layer	mm	0.1
$t_{c.g}$	Thickness of CTD-101K and glass-fiber layer	µm	50
$d_{c.i}$	Distance between strand and glass-fiber sleeve	µm	50
d_a	Distance between neighboring strands in the same layer	µm	50
d_c	Distance between neighboring strands in different layers	mm	0.1

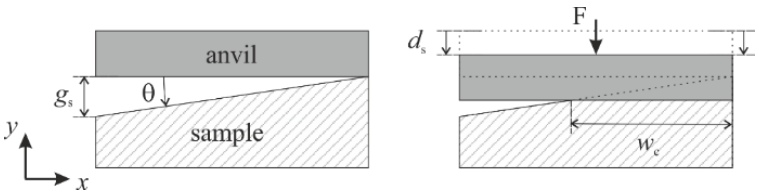

Figure 7. Schematic geometry of the compressed sample in the case of a non-zero misalignment angle θ.

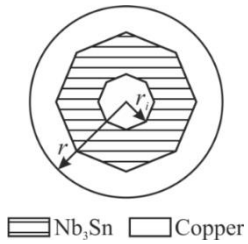

Figure 8. Layout of the refined strand model.

In reality, the strain concentration shown in Figure 6 can be expected to be even larger on a filament level. As discussed above, the models presented so far estimate the deviatoric strain in *homogeneous* Nb_3Sn cylindrical 'strands', not taking into account the internal strand composition. More detailed FE modelling by other authors shows that further stress- and strain- concentrations occur within the filamentary zone of the strands [21, 24, 25]. However, also without resorting to such detailed level of modelling, we can get an impression of the magnitude of this effect from a simplified model. The strain calculation with the cable model of Figure 5 was repeated, but this time replacing the homogeneous Nb_3Sn cylinders by strands modelled as in Figure 8. In this simple refinement, the 1 mm diameter strand is modelled as an octagonal uniform Nb_3Sn zone surrounded by a cylindrical copper matrix, and containing a central copper core. The Cu to non-Cu ratio of 1.22 is taken from the SMC-RRP strand. The diameter of the central copper core r_i is 200 μm. The Young's modulus and Possion's ratio of the copper are set to 137 GPa and 0.35 [21], respectively. Running the calculations of the model in Figure 2 again and comparing the average deviatoric strain in the filamentary zone of this refined strand model with the one in the homogeneous strand, reveals a further increase of $<\varepsilon_{dev}>$ with about 33%, as shown in Figure 9.

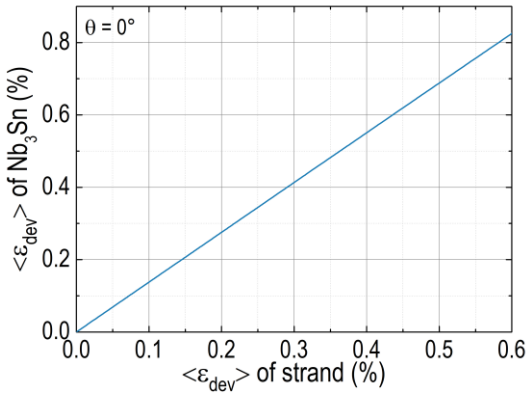

Figure 9. Average deviatoric strain in the filamentary zone of the refined strand model, plotted against the average deviatoric strain in the uniform strand model.

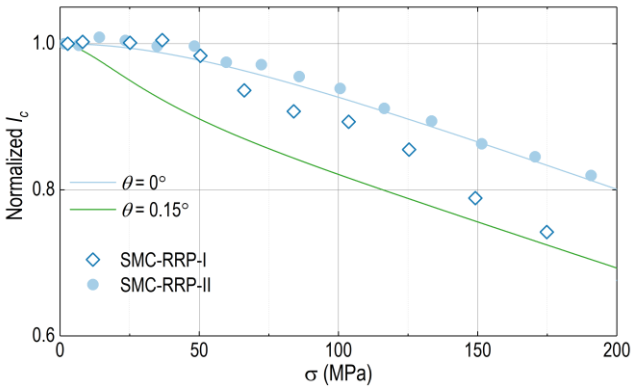

Figure 10. Normalized critical current versus transverse stress, illustrating the influence of a small misalignment angle on the pressure-dependence of the critical current.

The model outcomes presented in Figures 6 and 9 can now be combined with the strain scaling relation for the critical current density $J_c(T, B, \varepsilon)$ presented in the introduction, Equation (1) is applied to obtain a rough estimate of the effect of sample-anvil misalignment on the critical current measured in the press experiments [17]. Once more, we take an approach as simple as possible: the calculated average deviatoric strain in the filamentary zone of model strand 9 is inserted in Equation (1), using the characteristic scaling-law parameters given in Table 4, and it is assumed to dominate the overall pressure response of the critical current of the whole cable. Note that this is a rather crude approximation, neglecting possible effects of current redistribution among filaments or among strands and assuming that the magnetic peak-field location coincides with the region of maximum stress concentration. The result is shown as the solid lines in Figure 10. The top blue line is calculated for perfect alignment, when θ is 0°, while the bottom green curve is obtained with a misalignment angle θ of 0.15°. Strikingly, even this small misalignment causes a 13% lower I_c value at a transverse pressure of 200 MPa compared to the perfectly aligned case.

Table 4. SCALING-LAW PARAMETERS IN EQUATION (1) USED TO CALCULATE THE EFFECT OF STRAIN ON I_c [13].

Parameter	Description	Unit	Value
B_{c2}(4.2 K, 0)	Upper critical magnetic field at 4.2 K and zero strain	T	26.38
T_{c2}(0,0)	Critical temperature at zero field and strain	K	16.8
B	Applied magnetic field	T	11.63
T	Operation temperature	K	4.2
C_1	Scaling constant	AT/mm^2	46300
C_{dev}	Strain constant	-	1000
P	Low-field exponent of the pinning force	-	0.5
q	High-field exponent of the pinning force	-	2
e_{0d}	Residual strain component	%	0.09

The symbols in Figure 10 represent measurements on SMC-RRP cables, reported more extensively in [17]. Here we suffice to say that the only difference between the two cable experiments is the alignment impregnation that was applied to cable sample SMC-RRP-II but not to the identical cable SMC-RRP-I. The shape of the modeled $I_c(\sigma)$ curve when θ is 0.15° differs from the exact trend in the SMC-RRP-I data, but this is not too surprising given the crudeness of the mechanical and electrical models. However, at higher pressures the magnitude of the extra I_c reduction comparing the $\theta = 0.15°$ with the $\theta = 0°$ simulation is similar to the measured I_c difference between the cables SMC-RRP-I (without alignment impregnation) and SMC-RRP-II (with alignment impregnation). This suggests that the alignment impregnation is indeed effective in avoiding strain concentrations in the cable samples.

To investigate the effect of the alignment impregnation further, the calculations on the cable model of Figure 5 are repeated once more, but this time filling the gap between the anvil and the sample with a mixture of Stycast 2850FT and glass fiber, as shown in Figure 11. Note that this mixture is also used in actual alignment impregnation described in [17]. No literature data on the mechanical properties of a Stycast-glass mixture at 4.2 K were found. Instead, we used the data published in [26], reporting a Young's modulus of pure Stycast at 77 K in the range 22 to 29 GPa. To account for the lower temperature of 4.2 K and for the glass layers, we assume a high-end value of 30 GPa. Since also no published data were found for the Poisson's ratio, two extreme values are used: 0.1 and 0.4.

The average deviatoric strain values in the strands of this model are presented in Figure 12, including for comparison also the results without alignment impregnation previously shown in Figure 6. Both models were simulating a misalignment angle θ of 0.2°. Clearly, also in the simulations, the alignment impregnation virtually eliminates the effect of the misalignment angle, reducing the variation of the deviatoric strain between the strands to less than 1% and yielding a $<\varepsilon_{dev}>$ value that is near-identical to the one found for $\theta = 0°$.

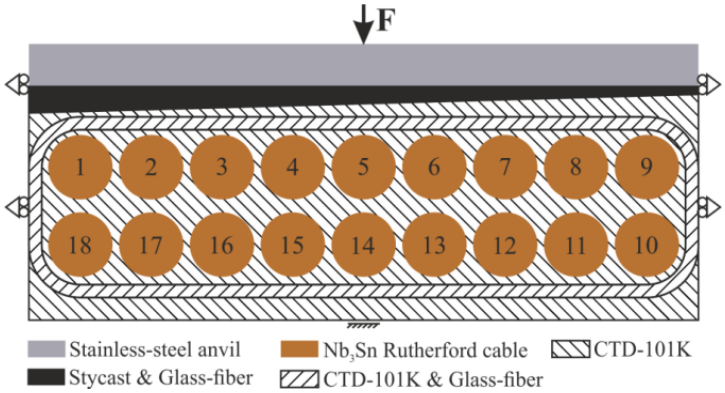

Figure 11. 2D mechanical model of the cable under transverse pressure, but now with and extra alignment impregnation to fill the gap between cable surface and anvil.

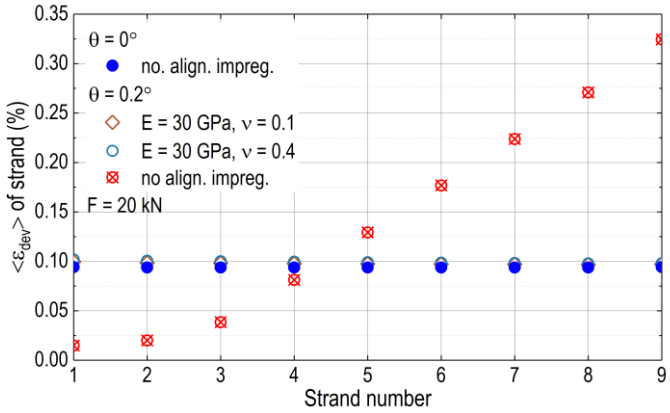

Figure 12. Average deviatoric strain in the strands 1-9 of the top cable face in Figure 5, with and without misalignment, and with and without alignment impregnation.

3. Conclusion

Simplified 2D FE modelling of impregnated and transversely loaded Nb_3Sn Rutherford cables shows that the average deviatoric strain acting on their strands decreases with increasing Young's modulus of the epoxy resin, as the resin carries an increasing part of the load. Also a larger Poisson's ratio of the resin, and therefore a larger bulk modulus, renders the stress on the strand more hydrostatic and thus reduces the deviatoric strain. Since the deviatoric strain of Nb_3Sn filaments has a direct impact on their critical current density, the use of a stiff and relatively incompressible epoxy resin significantly improves the pressure tolerance of the cables. The mechanical effect of an insulating glass sleeve around the cable, on the other hand, is relatively small.

The same type of mechanical model was also used to quantify the effect of a possible misalignment between the cable surface and the pressure anvil used in the cable experiments. For a typical Nb_3Sn cable layout, even a misalignment angle as small as 0.2° can cause a strain concentration by a factor 3 in the strands at the side of the cable that comes into contact with the anvil first. It should be noted that similar stress- and strain concentrations due to imperfect cable stacking may very well occur also in the winding pack of real magnets, which the experiment is designed to mimic. The alignment impregnation significantly improves the strain homogeneity in the transverse press experiments, rendering it essentially equal to the strain modelled for the perfectly aligned situation.

4. References

[1] Schoerling D *et al.* 2019 *IEEE Trans. Appl. Supercond.* **29**(5)
[2] Xu Q *et al.* 2016 *IEEE Trans. Appl. Supercond.* **26**(4)
[3] Marinozzi V, Bellomo G, Caiffi B, Fabbricatore P, Farinon S, Ricci A M, Sorbi M and Statera M 2018 *IEEE Trans. Appl. Supercond.* **28**(3)
[4] Kashikhin V V, Andreev N, Barzi E, Novitski I and Zlobin A V 2015 *Materials Science and Engineering, 101(conference 1)*
[5] Lorin C, Segreti M and Durante M 2018 *IEEE Trans. Appl. Supercond.* **28**(3)
[6] Toral F, Munilla J and Salmi T 2018 *IEEE Trans. Appl. Supercond.* **28**(3)
[7] Auchmann B, Brouwer L, Caspi S, Gao J, Montenero G, Negrazus M, Rolando G and Sanfilippo S 2018 *IEEE Trans. Appl. Supercond.* **28**(3)
[8] Bottura L and Bordini B 2009 *IEEE trans. Appl. Supercond.* **19**(3)
[9] Godeke A, Hellman F, Ten Kate H H J and Mentink M G T 2018 *Supercond. Sci. Technol.* **31**(10)
[10] Ten Haken B and Ten Kate H H J 1993 *Fusion Engineering and Design.* **20**
[11] Jewell M C, Lee P J and Larbalestier D C 2003 *Supercond. Sci. Technol.* **16**(9)
[12] Sadd M 2014 *Elasticity: theory, applications and numerics* (Academic Press) ISBN:978-0-12-408136-9
[13] Ten Haken B 1994 PhD dissertation, *University of Twente, The Netherlands*
[14] Calzolaio C, Mondonico G, Ballarino A, Bordini B, Bottura L, Oberli L and Senatore C 2015 *Supercond. Sci. Technol.* **28**(5)
[15] Van Oort J M 2000 PhD dissertation, *University of Twente, The Netherlands*
[16] Vallone G, Bordini B and Ferracin P 2018 *IEEE Trans. Appl. Supercond.* **28**(4)
[17] Gao P, Dhallé M, Bordini B, Ballarino A and Ten Kate H H J, to be published
[18] Gao P, Wessel W A J, Dhallé M, Otten S, Kario A, Van Nugteren J, Kirby G, Bottura L and Ten Kate H H J 2019 *Supercond. Sci. Technol.* **32**(5)
[19] Murtomaki J S, Van Nugteren J, Kirby G, Rossi L, Ruuskanen J and Stenvall A 2017 *IEEE Trans. Appl. Supercond.* **27**(4)
[20] Bauer P, Rajainmaki H and Salpietro E 2007 *Inside document of CERN*
[21] Calzolaio C, Mondonico G, Ballarino A, Bordini B, Bottura L, Oberli L and Senatore C 2015 *Supercond. Sci. Technol.* **28**(5)
[22] CTD-101K 2014 *Composite Technology Development, Lafayette, CO, USA*
[23] Otten S, Dhallé M, Gao P, Wessel W, Kario A, Kling A and Goldacker W 2015 *Supercond. Sci. Technol.* **28**(6)
[24] Daly M, Loffler C H, Smekens D, Fontenla A T, De Frutos O S, Guinchard M and Savary F 2018 *IEEE Trans. Appl. Supercond.* **28**(3)
[25] Zhai Y, D'Hauthuille L, Barth C and Senatore C 2016 *IEEE Trans. Appl. Supercond.* **26**(4)
[26] Kirby G A *et al.* 2016 *IEEE Trans. Appl. Supercond.*, **26**(3)

Acknowledgments

The work presented in this paper was done in the frame of the EuroCirCol project, partially funded by EU's H2020 framework program under grant agreement no. 654305.